Journal of
Materials Chemistry B

Accepted Manuscript

This article can be cited before page numbers have been issued, to do this please use: D. Masram, N. K. K. Mogha, V. sahu and R. K. Sharma, *J. Mater. Chem. B*, 2018, DOI: 10.1039/C8TB01604F.

ROYAL SOCIETY OF CHEMISTRY

rsc.li/materials-b

View Article Online
DOI: 10.1039/C8TB01604F

Reduced graphene oxide nanoribbon immobilized gold nanoparticles based electrochemical DNA biosensor for detection of *Mycobacterium tuberculosis*

Navin Kumar Mogha, Vikrant Sahu, Raj Kishore Sharma*, Dhanraj T. Masram*

Department of Chemistry, University of Delhi, Delhi-110007, India

Abstract

Tuberculosis is one of the most dreadful disease caused by *Mycobacterium tuberculosis* with more than 9 million individuals suffering from it in 2014. Traditional methods of detection are not efficient enough for its quick and reliable detection, therefore, it becomes imperative to develop methods of its detection in the early stage. Consequently, we report a highly sensitive and selective biosensor for detection of *Mycobacterium tuberculosis*. In this work, Gold nanoparticles (AuNPs, dia.~6 nm, 1.81 wt.% loading) are immobilized over reduced graphene oxide nanoribbons (RGONRs). ssDNA/Au/RGONR electrode is prepared by immobilizing Au nanoparticles followed by covalent modification of Au nanoparticles with 5'SH-ssDNA. As per the best knowledge of authors, target DNA of *Mycobacterium tuberculosis* is detected using ssDNA/Au/RGONR bioelectrode by cyclic voltammetry and chronoamperometric methods for the first time. With high detection efficiency (0.1fM), ssDNA/Au/RGONR bioelectrode exhibited better signal amplification and electrochemical response as compared to bare Au and RGONR electrodes. Additionally, ssDNA/Au/RGONR bioelectrode displayed good linear response to different concentrations of target *M. tuberculosis* DNA. ssDNA/Au/RGONR has shown excellent specificity (92%) to *Mycobacterium tuberculosis* target DNA as compared with non-complementary DNA. Au/RGONR matrix has a potential be used as immobilization

View Article Online
DOI: 10.1039/C8TB01604F

platform for single-stranded probe DNAs of different other diseases other than Tuberculosis reported here.

Keywords: - *Mycobacterium tuberculosis;* biosensor; DNA; Graphene oxide.

1. Introduction

Tuberculosis (TB) is one of the most deadly infectious disease caused by bacteria *Mycobacterium tuberculosis (M. tuberculosis)* from which about 9.6 million people were infected worldwide in 2014[1]. Conventional diagnostic methods for TB detection such as polymerase chain reaction (PCR) and restriction fragment length polymorphism (RFLP), are often time-consuming and require trained expertise for operation. Therefore, there is an urgent need for the development of a quick, sensitive, reliable and specific method for *M. tuberculosis* detection.

In this context, development of highly sensitive and efficient biosensors for detection of numerous analytes are possible by the advancements in molecular bioelectronics[2–7]. DNA, or deoxyribonucleic acid, is a hereditary material in humans and almost all other organisms consisting of the double helix of nucleotides. DNA sensors follows working principal based on hybridization of the single-stranded probe DNA with target complementary DNA sequences. These sensors are extensively used in the diagnosis of various diseases like gene sequences analysis, forensics and medical treatment assessments[8–12]. Electrochemical DNA sensors are particularly attractive among various DNA based sensors owing to their simplicity, low cost, miniaturization, high specificity and sensitivity[13–15]. Recently, various electrochemical DNA biosensors are reported for the detection of different analytes and diseases such as E.Coli[16],

View Article Online
DOI: 10.1039/C8TB01604F

Breast Cancer[17], HIV[18], Typhoid[2], Bacterial Meningitis[19], and Human Papillomavirus[20], Aeromonas hydrophila[21].

Nanomaterials in electrochemical DNA biosensors are used to increase the performance of point-of-care diagnostics in biomedical applications like efficient immunoassays, enhanced sensitivity in enzymatic biosensors and electrochemical DNA detection[22]. Nanomaterials are well known for the characteristics like increased surface to volume ratio, increased electron transfer, surplus binding sites with enhanced biocompatibility and higher signal intensities in contrast to their bulk counterparts used in electrochemical sensors[23–25]. Biosensors based on diverse nanomaterials, for instance, gold, silver, zinc oxide, carbon nanomaterials (Graphene, Graphene Oxide (GO), Carbon Nanotubes (CNTs), Fullerenes etc.), iron oxide and their composites have been extensively reported. Gold, modified GCE, CNT and graphene-coated electrodes have been used for DNA immobilization[26–29].

Graphene is a honeycomb (2D) lattice of sp^2 hybridized carbon atoms[30–33] whose properties are significantly depends upon the synthetic procedure like mechanical synthesis or chemical synthesis[34,35]. Functionalized graphene in bulk can be synthesized using chemical routes, however, the control over its structure and lattice defects is compromised compared to graphene obtained from Mechanical or Physical methods of synthesis[36]. On the other hand, lattice defects and edges in graphene are shown to enhance its performance in various applications [37]. Graphene oxide nanoribbons (GONRs) are very promising analogs of graphene with rich edge chemistry compared to pristine graphene. Recent reports on longitudinal unzipping of CNTs by strong oxidizing agents[38,39]suggest, that the defects and edge density in graphene significantly improve the properties like electronic conduction and catalytic performance, moreover the defects are also shown to bring ferromagnetism in graphene[40].

View Article Online
DOI: 10.1039/C8TB01604F

Beside defects, functional groups present on graphene increases their reactivity, solubility in water and polar solvents along with the electrochemical responses [41]. This increment in reactivity is resulted due to adsorption of molecules via π–π stacking interaction as well as by hydrogen bonding or electrostatic interactions with functional groups present over edges[42].

Noble metal nanoparticles like Au nanoparticles (AuNPs) are used as electrochemical biosensors and a synergistic effect is noticed for example in chitosan/rGO/AuNPs modified Pt electrode for electrochemical glucose biosensor [43], DNAzyme modified AuNPs/GO nanocomposites based lead ion biosensor[44]. DNA biosensors based on hybridization of probe and target single-stranded DNA by immobilizing DNA over AuNPs have also been reported previously [45,46].

As stated above, GONR, due to its graphene like structure and rich edge chemistry improves the electronic conduction. Moreover, it is also reported that AuNPs along with nanocarbon helps in amplification of the signals[47,48]. Therefore, in the present article, a DNA biosensor based upon AuNPs immobilized, reduced GONRs (Au/RGONR) for the ultra-sensitive detection of *Mycobacterium tuberculosis* is reported. GONR is synthesized as per procedure reported elsewhere[49] followed by in situ immobilization of AuNPs on GONR. Electrochemical detections, based on the Hybridization of the Au/RGONR immobilized Probe Single-stranded DNA with target single-stranded DNA of *M. tuberculosis* showed many order of magnitude higher detection efficiency for *M. tuberculosis* DNA.

View Article Online
DOI: 10.1039/C8TB01604F

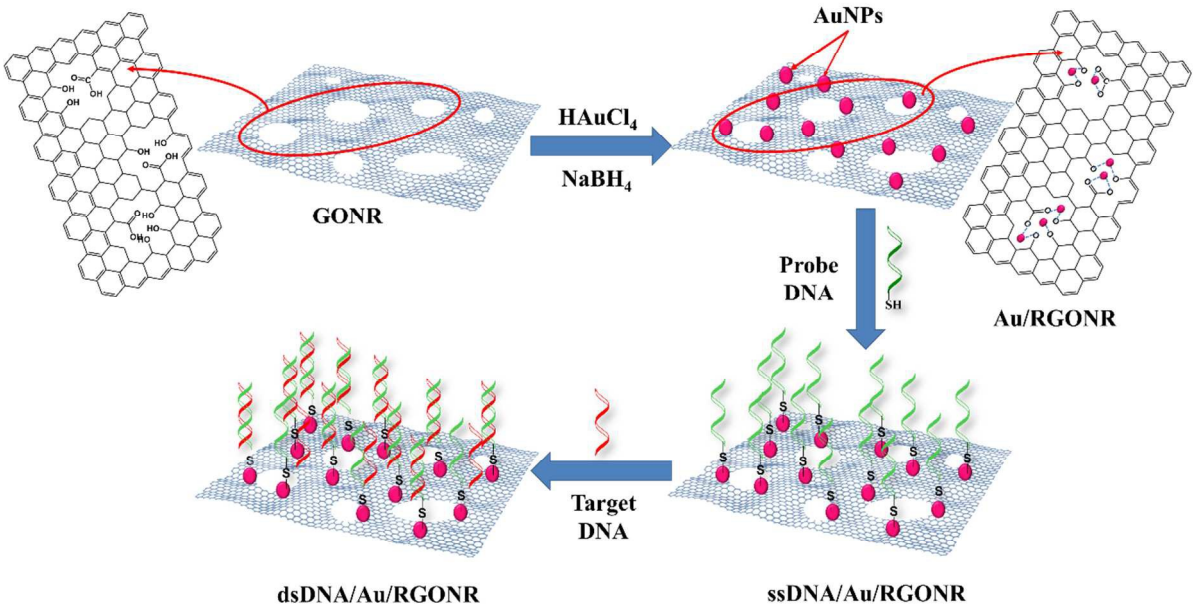

Scheme 1 Schematic representation of the synthetic procedure and principal of detection

2. Materials and Methods

2.1 Materials

Multi-walled carbon nanotubes (Length- 10-30µm, OD- 30-50nm), $HAuCl_4.3H_2O$ were obtained from SRL, India. Oligonucleotide probe sequence specific to *M. Tuberculosis*, complementary target, one-base mismatch, and noncomplementary DNA have been procured from Sigma-Aldrich, India. All solutions were prepared in deionized (DI) water.

Oligonucleotide sequences used in this work are:

Thiolated probe: SH-5'-GGTCTTCGTGGCCGGCGTTCA-3'

Complementary: 5'-TGAACGCCGGCCACGAAGACC-3'

One-base mismatch: 5'-TGAACGCCGACCACGAAGACC-3'

Noncomplementary: 5'-ATGTCTCAAGCCAGCTGCTG-3'

View Article Online
DOI: 10.1039/C8TB01604F

2.2 Characterization techniques

X-ray diffraction patterns were recorded using X-ray diffractometer (Model No. D8 DISCOVER). Morphological characterization was carried out using TECNAI 200 kV TEM (Fei, Electron Optics) equipped with digital imaging and 35 mm photography system. Electrochemical characterization was carried out using a CH-604D electrochemical workstation. Raman spectrums were recorded by Renishaw InVia Reflex Micro-Raman spectrometer in which the sample was excited by 514 nm wavelength Ar^+ laser.

2.3Synthesis of GO and GONR

GO was synthesized by previously reported method [24].GONR was synthesized by chemical unzipping of MWCNTs using the procedure reported previously with slight modifications[49]. Briefly,1.5g of MWCNTs was added to 200ml H_2SO_4/H_3PO_4 (11:1) solution under stirring for 1 h (until mixture becomes homogenous) followed by the addition of 9g $KMnO_4$ slowly to the reaction mixture under continuous stirring at 80 °C for 12 h. After cooling, the reaction mixture was filtered, washed with water and ethanol successively and then dried in vacuum.

2.4 Synthesis of Au/RGONR

200mg GONR was dispersed in 100ml DI water using sonication until homogenization. Subsequently, 5ml $HAuCl_4$ solution (3mM) was added followed by sonication for 15 min. Resulting dispersion was ice-cooled and 100µl of 0.1M $NaBH_4$ was added dropwise to synthesize AuNPs over the surface of GONR. Dark black reaction mixture so obtained was filtered, washed with Deionized water till pH of filtrate becomes neutral, and dried in vacuum.

2.5 Preparation of ssDNA/Au/RGONR Electrode

View Article Online
DOI: 10.1039/C8TB01604F

Indium Tin Oxide (ITO) coated glass was used as a substrate for electrode preparation. Firstly, a film of Au/RGONR was prepared using spray deposition of Au/RGONR 10mg/ml dispersion onto pre-cleaned ITO glass, followed by drying at 60 °C for 4h. Afterward, 5'SH-ssDNA probe was covalently attached to the surface of the electrode by Au-S binding. Au/RGONR electrode was incubated after drop casting 10µl of a 1µM solution of probe 5'SH-ssDNA for 1h at room temperature. The formed electrode was washed with water to remove excess of unbound DNA and stored at 4 °C for further use up to three weeks.

3. Results and Discussions

3.1 Raman and XRD Analysis

Raman spectra of GO, GONR and Au/RGONR are shown in Fig. 1(a). GO exhibiting characteristic D band at 1350 cm^{-1} and G band at 1590 cm^{-1}. The D peak in graphene is resulted due to breathing mode j-point phonons of A1g symmetry of sp^3 bonded carbon atoms in disordered graphene while G peak is assigned due to first order scattering of E_2g phonons in sp^2 bonded carbon atoms[50]. Presence of oxygenated functionalities in GONR increases disorders in sheet structure, as a result of which G peak was observed at 1601 cm^{-1} slightly higher than GO [50]. I_d/I_g ratio exhibited an increment of 0.79, 0.90 and 0.92 respectively for GO, GONR and Au/RGONR samples indicating increased disorderness. Increase in I_d/I_g ratio from GO, GONR is attributed to the structural defects generated as a consequence of increased edge density. A further increase is credited to the immobilization of Au nanoparticles on GONR surface, that by the action of $NaBH_4$ undergo reduction to RGONR. Presence of 2D band in GONR and Au/RGONR spectra indicate the existence of multiple stacked graphitic layers. Figure 1 (b), the XRD patterns of GO, GONR, and Au/RGONR demonstrate typical crystal planes peaking at 2Θ = 11.4 and 10.3 due to <001> crystal planes of GO and GONR respectively. While peaks at 2Θ =

View Article Online
DOI: 10.1039/C8TB01604F

42.28 exhibit the presence of <100> crystal plane of GO and GONR. Presence of comparatively more oxidative environment is the reason of lower 2Θ value for <001> plane in GONR. XRD pattern of Au/RGONR consists of five peaks typically at 2Θ = 25.36 is due to <002> crystal plane of RGONR, whereas 2Θ = 38.11, 44.3, 64.57 and 77.54 indicating existence of <111>, <200>, <220> and <311> planes of Au nanoparticles.

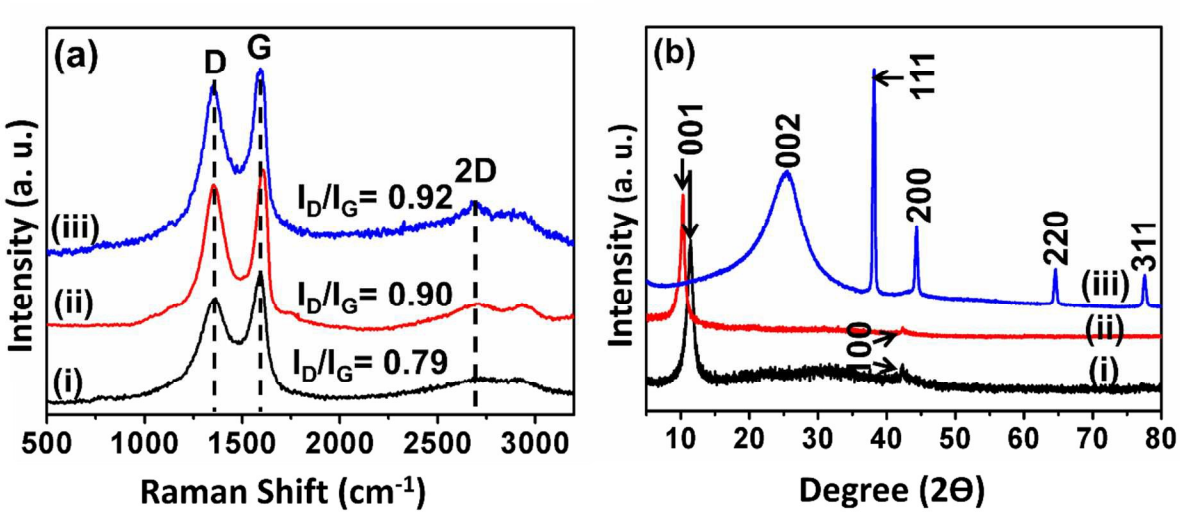

Fig. 1 (a) Raman spectra and (b) XRD patterns of (i) GO (ii) GONR (iii) Au/RGONR

3.2 Morphological features

Figure 2, depicts the morphological features of GONR and Au/RGONR along with SAED pattern of Au/GONR and Au nanoparticle distribution over RGONR surface. TEM micrograph in Fig. 2 (a), shows the mass distribution of GONR from MWCNTs unzipping reaction while overlapped completely unzipped GONRs resembling graphene sheets can be seen in Fig. 2 (b). Furthermore, Fig. 2 (c) portrays, uniformly immobilized Au nanoparticles over RGONR surface. Since the Au NPs imparts high contrast, structural details of overlapped RGONR are not completely visible. Selected Area Electron Diffraction (SAED) pattern for Au/RGONR in Fig. 2 (d), presents <002> crystal plane of RGONR, <111> and <220> crystal planes of Au

View Article Online
DOI: 10.1039/C8TB01604F

nanoparticles and correlate it with the X-ray diffraction pattern of Au/RGONR. Fig. 2 (e), shows the size distribution of Au nanoparticles on RGONR surface with an average size of 6 nm. Energy-dispersive X-ray (EDX) analysis of Au/RGONR in Fig. 2 (f) confirm the presence of Au in Au/RGONR, also elemental percentage of carbon, oxygen and gold is tabulated in Table S1 showing loading of Au about 1.81% .

View Article Online
DOI: 10.1039/C8TB01604F

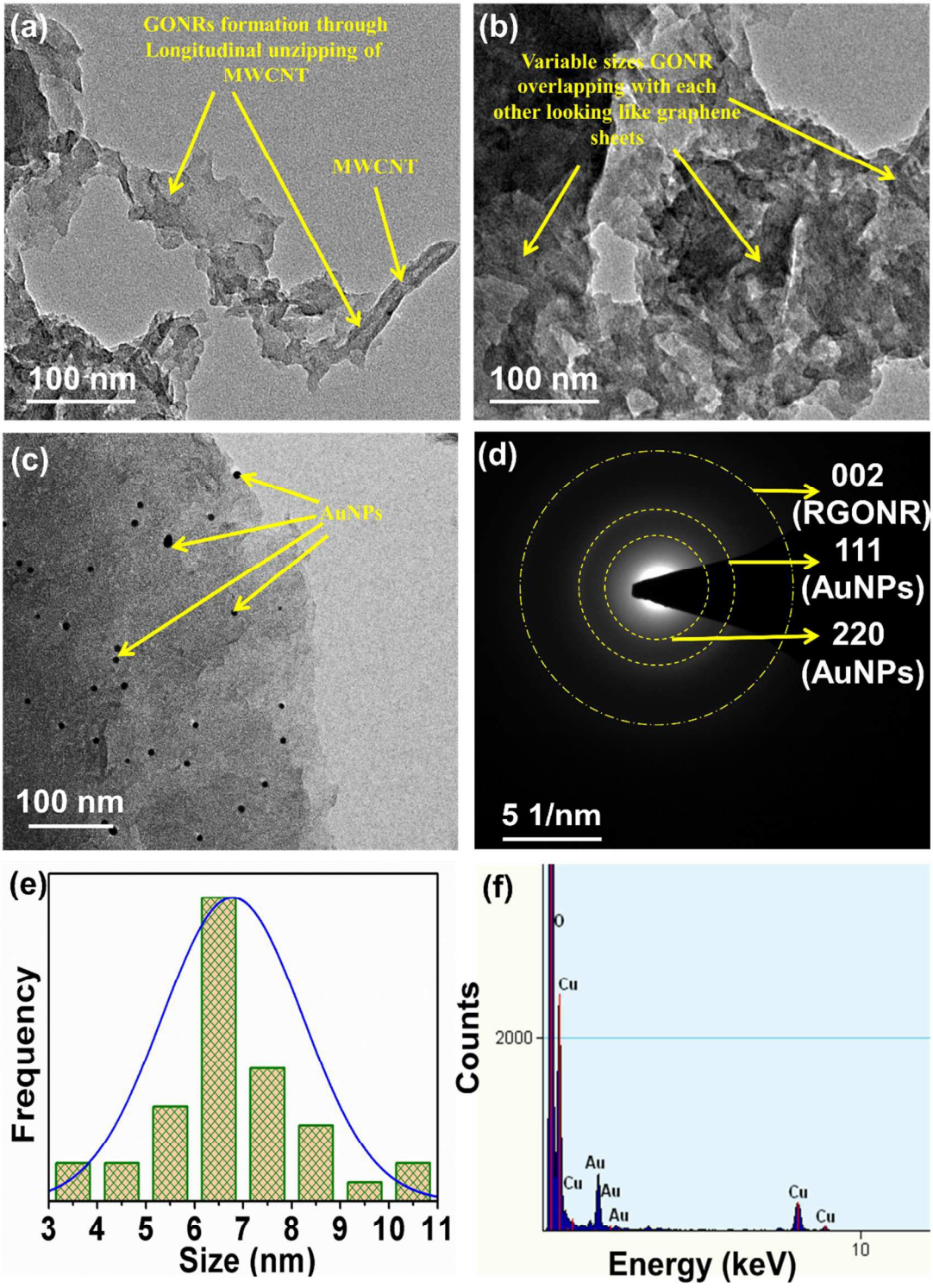

Figure 2, TEM micrographs of (a) GONR formation from MWCNT (b) Overlapped GONRs resembling like graphene sheets (c) Au/RGONR (d) SAED pattern of Au/RGONR and(e) size distribution of Au nanoparticles over RGONR surface (f) EDX pattern for Au/RGONR

View Article Online
DOI: 10.1039/C8TB01604F

3.3 Electrochemical Characterization

Figure 3(a) provides the comparison among the cyclic voltammograms recorded on bare ITO, Au/RGONR, ssDNA/Au/RGONR and dsDNA/Au/RGONR as working electrodes. Each electrode shows well-defined redox peaks with a significant increase in redox peak current from bare ITO electrode to Au/RGONR. The increase in peak current for bare ITO electrode to Au/RGONR is attributed to fast electron-transfer ability of RGONR due to its edge chemistry[49] and good conductivity of uniformly distributed Au nanoparticles upon RGONR surface[43]. Furthermore, it is reported that conductivity of AuNPs is size dependent, lesser the size more is conducting nature of AuNPs[48]. Additionally, more concentration of Au salt will lead to the formation of larger size AuNPs[51], hence in current work, small size AuNPs are synthesized with less density to get uniformly distributed AuNPs over RGONR. Additionally, Figure S1, Comparative Cyclic voltammograms for bare ITO, Au/RGONR/ITO, RGONR/ITO and AuNPs/ITO electrodes in Zobell's Solution at scan rate of 50 mVs^{-1}, revealing Au/RGONR/ITO electrode have better conductive performance as compared to others to be utilized as platform for DNA immobilization. Furthermore, it is already reported in literature that AuNPs when immobilized on CNT modified electrode its conductivity increased many folds while attached to macromolecule, as compared to immobilized on bare electrode[47], which is supporting current studies. Hence, present Au/RGONR/ITO matrix providing better signal amplification as compared to bare ITO, and RGONR/ITO electrodes, and therefore better the biosensing performance.

View Article Online
DOI: 10.1039/C8TB01604F

However, a considerable decrease in peak current for ssDNA/Au/RGONR is noted with respect to Au/RGONR, which further decreased in case of dsDNA/Au/RGONR. This decrease is attributed to the electrostatic repulsion between the negatively charged phosphate backbone of DNA covalently attached to Au/RGONR matrix and $[Fe(CN)_6]^{3-/4-}$ moieties present in Zobell's solution, rendering a slow electron transfer kinetics. Figure 3(b) exhibits the relationship between the amount of 5'SH-ssDNA probe used and hybridization percentage with target DNA. It suggests that 10 µl ssDNA sufficient for more than 50% hybridization.

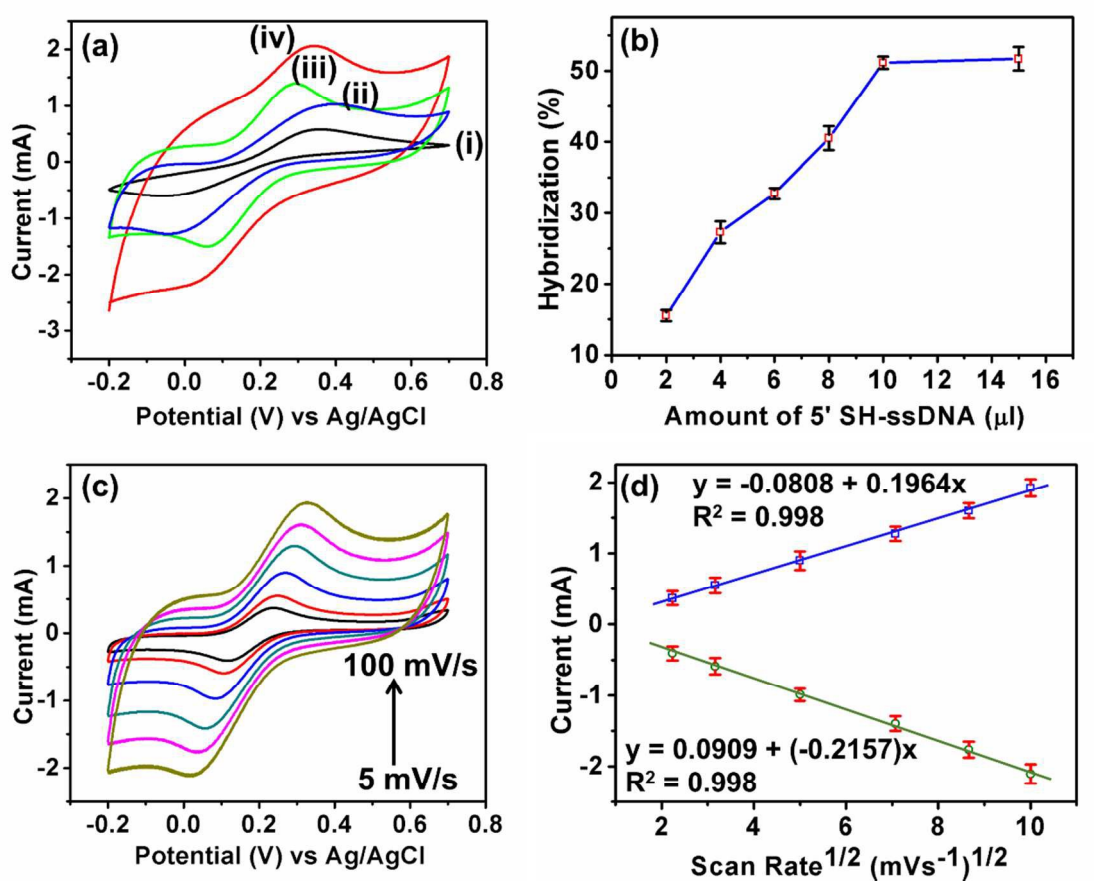

Figure 3, (a) Cyclic voltammograms for (i) bare ITO (ii) dsDNA/Au/RGONR (iii) ssDNA/Au/RGONR (iv) Au/RGONR electrodes in Zobell's Solution at scan rate of 50 mVs^{-1}(b) optimization of 5'SH-ssDNA amount for hybridization studies (c) Cyclic voltammograms of ssDNA/Au/RGONR electrode at different scan rates in Zobell's solution (d) Linear relationship between redox peak currents and square root of scan rate suggesting diffusion-controlled process

View Article Online
DOI: 10.1039/C8TB01604F

Cyclic voltammograms of ssDNA/Au/RGONR bioelectrode recorded at different scan rates are represented in Figure 3 (c). A continuous increase in peak current for both anodic and cathodic scans with increasing scan rate is observed. Furthermore, redox peak currents exhibit a linear relationship with square root of scan rate (Figure 3 (d)) signifying a diffusion controlled process taking place at modified electrode[52]with linear regression equation y = -0.0808 + 0.1964x; R^2 = 0.998 and y= 0.0909 + (-0.2157) x; R^2 = 0.998 for anodic and cathodic peak currents respectively. Here y is peak current (mA), x is square root of scan rate [$(mVs^{-1})^{1/2}$] and R is regression coefficient.

Figure 4(a) exhibit DNA hybridization studies performed for detection of *Mycobacterium tuberculosis* using cyclic voltammetry in Zobell's solution without any redox indicator. A continuous decrease in redox peak current is observed with increase in target DNA concentration (from 0.1fM to 10^{-6} M). This decrease can be credited to the increase in electrostatic repulsion between negatively charged phosphate backbone of DNA and $[Fe(CN)_6]^{3-/4-}$moieties present in the electrolyte solution. Decline of redox peak current exhibit a linear relationship with concentrations of target DNA present in solution (Figure 4 (b)) following the regression equations y = 0.352 + (-0.0524) x; R^2 = 0.950 and y = -0.4836 + 0.0570x; R^2 = 0.975 for anodic and cathodic peak current respectively. Similar results are also obtained when the same experiment is performed by chronoamperometry (Figure 4 (c)). An incessant decrease in current with different concentrations of target DNA alongtime correlates our findings with cyclic voltammetry results. Figure 4 (d) shows the gradual increase in hybridization percentage as the concentration of target DNA increases ranging from about 10.6% to 51.3% for 0.1fM to 10^{-6} M respectively.

View Article Online
DOI: 10.1039/C8TB01604F

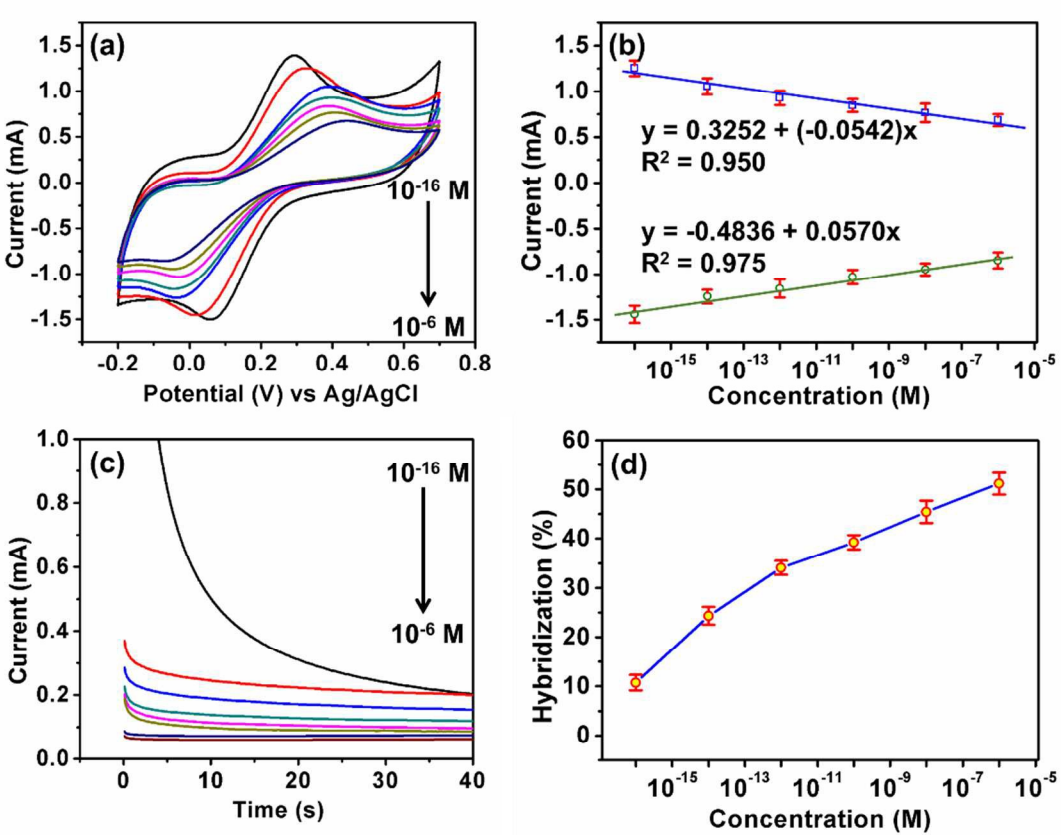

Figure4 (a) Cyclic voltammograms showing DNA hybridization studies with different concentrations of target DNA (b) Linear relationship between target DNA concentration and redox peak current (c) Chronoamperometric analysis of DNA hybridization experiment (d) DNA hybridization percentage with respect to target DNA concentrations

Figure 5 demonstrates the specificity and selectivity of ssDNA/Au/RGONR electrode towards DNA of *Mycobacterium tuberculosis.* Almost negligible hybridization of probe ssDNA observed with non-complementary DNA while it increases up to more than 51% in case of target DNA belonging to *Mycobacterium tuberculosis* resulting in a specificity of more than 92%. If only one base pair is mismatched in target DNA than a drastic decrease of about 9% hybridization is noted suggesting excellent specificity and selectivity towards *Mycobacterium tuberculosis* target DNA, as a mismatch of the only single base pair is almost impossible for microbes responsible for two different diseases.

View Article Online
DOI: 10.1039/C8TB01604F

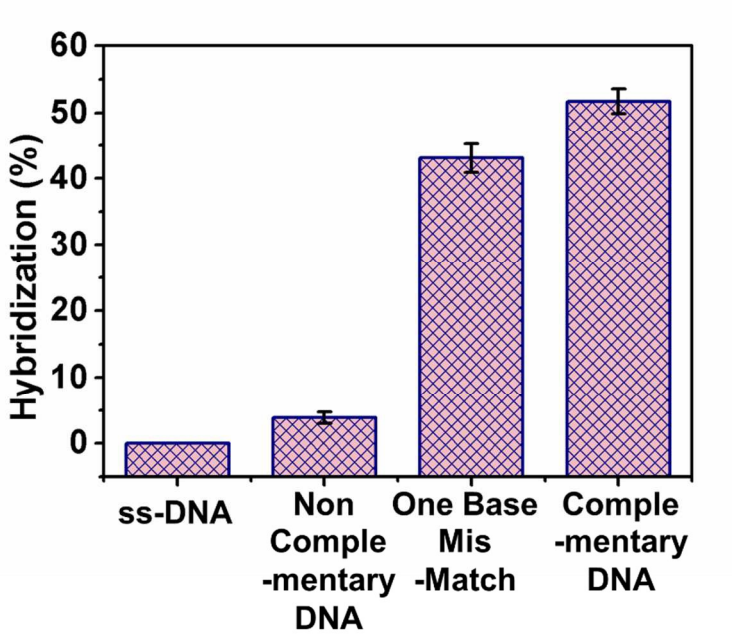

Figure 5 Specificity and selectivity of ssDNA/Au/RGONR bioelectrode towards target DNA of *Mycobacterium tuberculosis*

3.4 Mechanism of Detection

Scheme 2, explains the mechanism of detection by ssDNA/Au/RGONR bioelectrode. Blue colored arrows representing electron transfer kinetics which is more in Au/RGONR but decreases in ssDNA/Au/RGONR and dsDNA/Au/RGONR due to repulsion between negatively charged phosphate backbone of DNA and $[Fe(CN)_6]^{3-/4-}$ions in the electrolyte. While red colored arrows indicating an increase in repulsion in dsDNA/Au/RGONR due to DNA hybridization. Hence, when ssDNA is immobilized over Au/RGONR a slight decrease in electron transfer rate is observed, while it further decreases when hybridization starts with complementary target ssDNA to form dsDNA/Au/RGONR. This rate of electron transfer continues to decrease with increase in the concentration of complementary target ssDNA.

View Article Online
DOI: 10.1039/C8TB01604F

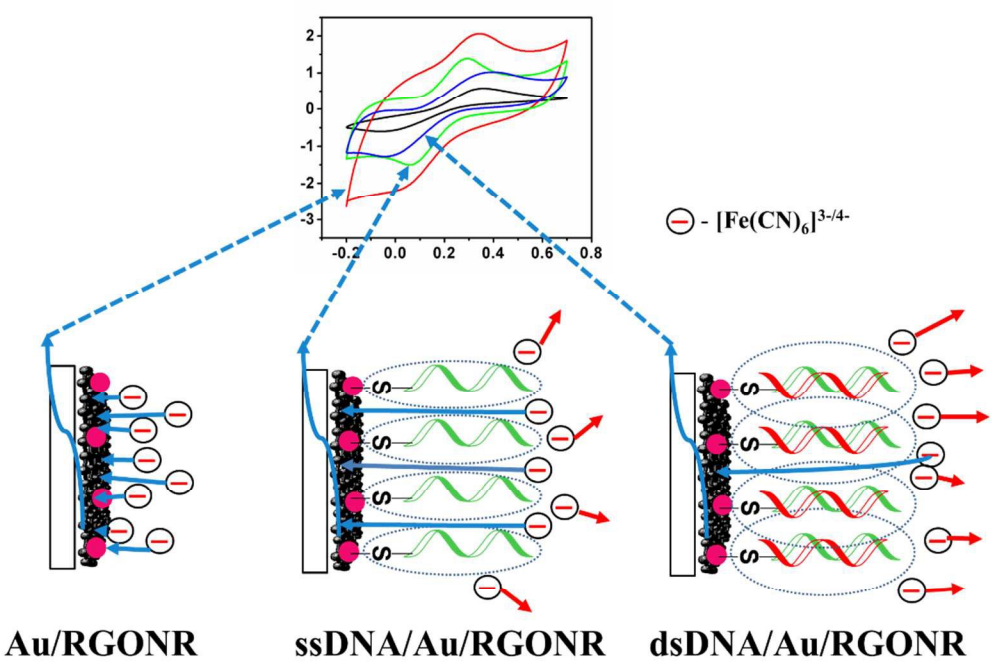

Scheme2 Mechanism of detection by ssDNA/Au/RGONR bioelectrode

4. Conclusion

We reported a highly sensitive, and specific electrochemical DNA biosensor based upon the AuNPs immobilized reduced GONRs for detection of *Mycobacterium tuberculosis*. Even trace amount of (0.1fM) of target DNA is detected with ssDNA/Au/RGONR electrode. These values are superior to the literature reports till date (Table 1). ssDNA/Au/RGONR has been found to be more than 92% specific to target DNA as compared with other non-complementary DNA. In this work, Au nanoparticles are immobilized over GONR surface for in situ syntheses of Au/RGONR followed by covalent modification of Au nanoparticles with 5'SH-ssDNA probe which is used as probe material for detecting *Mycobacterium tuberculosis* target DNA. Although it is not possible to reuse ssDNA/Au/RGONR bioelectrode, but Au/RGONR matrix have potential for immobilization of other probe DNAs for detection of different deadly diseases such as typhoid, and diverse kind of cancers etc.

View Article Online
DOI: 10.1039/C8TB01604F

Table 1 Comparison of the reported biosensors with present work

S.No.	Electrode Material	Detection Technique	Detection Limit	Reference
1.	Au Nanoparticles	Electrochemical	1.25ng/ml	[53]
2.	Gold electrode	Impediometry	1nM	[54]
3.	Quantum dots/polymer	Square wave voltammetry	1fM	[18]
4.	Dextrin coated Au nanoparticles	Differential Pulse voltammetry	0.01ng/µl	[55]
5.	ZrO_2/Gold electrode	Differential Pulse voltammetry	0.065ng/µl	[56]
6.	MWCNTs/PPy/PAMAN/Ferrocene	Cyclic Voltammetry	0.3fM	[57]
7.	Au/RGONR	Cyclic Voltammetry, Chronoamperometry	0.1fM	Present work

Conflicts of interest

There are no conflicts to declare for authors.

Acknowledgments

Authors are grateful to the University of Delhi, Delhi, India for providing financial assistance through R & D fund and Sophisticated Analytical Instrument Facility (SAIF) – AIIMS, New Delhi, under the SAIF Program of DST for providing TEM facility. V. Sahu greatly acknowledges CSIR (Council of Scientific & Industrial Research) for providing SRF.

References

View Article Online
DOI: 10.1039/C8TB01604F

1 World Health Organization (WHO), .

2 A. Singh, G. Sinsinbar, M. Choudhary, V. Kumar, R. Pasricha, H. N. Verma, S. P. Singh and K. Arora, *Sensors Actuators, B Chem.*, 2013, **185**, 675–684.

3 K. Arora, S. Chand and B. D. Malhotra, *Anal. Chim. Acta*, 2006, **568**, 259–274.

4 S. K. Arya, S. Saha, J. E. Ramirez-Vick, V. Gupta, S. Bhansali and S. P. Singh, *Anal. Chim. Acta*, 2012, **737**, 1–21.

5 K. Ariga, Q. Ji, J. P. Hill, Y. Bando and M. Aono, *NPG Asia Mater.*, 2012, **4**, e17.

6 A. Bétard and R. A. Fischer, *Chem. Rev.*, 2012, **112**, 1055–1083.

7 P. Lin and F. Yan, *Adv. Mater.*, 2012, **24**, 34–51.

8 E. Palecek, M. Fojta, M. Tomschik and J. Wang, *Biosens. Bioelectron.*, 1998, **13**, 621–628.

9 J. Wang, D. Xu, A. N. Kawde and R. Polsky, *Anal. Chem.*, 2001, **73**, 5576–5581.

10 J. Wang, D. Xu, A. Erdem, R. Polsky and M. A. Salazar, *Talanta*, 2002, **56**, 931–938.

11 L. Wang, A. Wu and G. Wei, *Analyst*, 2018, **143**, 1526–1543.

12 L. Wang, Y. Zhang, A. Wu and G. Wei, *Anal. Chim. Acta*, 2017, **985**, 24–40.

13 H. Cai, Y. Wang, P. He and Y. Fang, *Anal. Chim. Acta*, 2002, **469**, 165–172.

14 J. Wang, *Biosens. Bioelectron.*, 2006, **21**, 1887–1892.

15 M. Gerard, A. Chaubey and B. D. Malhotra, *Biosens. Bioelectron.*, 2002, **17**, 345–359.

16 Y. Du, S. Guo, S. Dong and E. Wang, *Biomaterials*, 2011, **32**, 8584–8592.

17 P. A. Rasheed and N. Sandhyarani, *Sensors Actuators, B Chem.*, 2014, **204**, 777–782.

18 Z. Yan, N. Gan, H. Zhang, D. Wang, L. Qiao, Y. Cao, T. Li and F. Hu, *Biosens. Bioelectron.*, 2015, **71**, 207–213.

19 M. Tak, V. Gupta and M. Tomar, *Biosens. Bioelectron.*, 2014, **59**, 200–207.

View Article Online
DOI: 10.1039/C8TB01604F

20 H. Huang, W. Bai, C. Dong, R. Guo and Z. Liu, *Biosens. Bioelectron.*, 2015, **68**, 442–446.

21 M. Ligaj, M. Tichoniuk, D. Gwiazdowska and M. Filipiak, *Electrochim. Acta*, 2014, **128**, 67–74.

22 X. Zhang, Q. Guo and D. Cui, *Sensors*, 2009, **9**, 1033–1053.

23 J. Wang, *Analyst*, 2005, **130**, 421.

24 N. K. Mogha, V. Sahu, M. Sharma, R. K. Sharma and D. T. Masram, *Appl. Biochem. Biotechnol.*, , DOI:10.1007/s12010-014-0986-z.

25 N. Mogha, V. Sahu, M. Sharma, R. Kishore and D. T. Masram, *JMADE*, 2016, **111**, 312–320.

26 P. He, Y. Xu and Y. Fang, *Anal. Lett.*, 2005, **38**, 2597–2623.

27 F. Lucarelli, S. Tombelli, M. Minunni, G. Marrazza and M. Mascini, *Anal. Chim. Acta*, 2008, **609**, 139–159.

28 L. Feng, Y. Chen, J. Ren and X. Qu, *Biomaterials*, 2011, **32**, 2930–2937.

29 K. Jayakumar, R. Rajesh, V. Dharuman, R. Venkatasan, J. H. Hahn and S. Karutha Pandian, *Biosens. Bioelectron.*, 2012, **31**, 406–412.

30 N. Mogha, S. Kirti and D. T. Masram, *J. Nanosci. Nanotechnol.*, 2017, **17**, 2508–2514(7).

31 N. Mogha, S. Gosain and D. T. Masram, *Appl. Surf. Sci.*, , DOI:10.1016/j.apsusc.2016.11.182.

32 A. S. Dobrota, I. A. Pašti, S. V. Mentus, B. Johansson and N. V. Skorodumova, *Electrochim. Acta*, 2017, **250**, 185–195.

33 A. K. Geim and K. S. Novoselov, *Nat. Mater.*, 2007, 183–191.

34 C. Cui, J. Huang, J. Huang and G. Chen, *Electrochim. Acta*, 2017, **258**, 793–799.

35 T. Kuila, S. Bose, A. K. Mishra, P. Khanra, N. H. Kim and J. H. Lee, *Prog. Mater. Sci.*,

View Article Online
DOI: 10.1039/C8TB01604F

2012, **57**, 1061–1105.

36 R. S. Park, S.; Ruoff, *Nat. Nanotechnol.*, 2009, **4**, 217–224.

37 V. Sahu, S. Goel, A. Kumar Tomar, G. Singh and R. K. Sharma, *Electrochim. Acta*, 2017, **230**, 255–264.

38 V. Sahu, S. Goel, R. K. Sharma and G. Singh, *Nanoscale*, 2015, **7**, 20642–20651.

39 D. V Kosynkin, A. L. Higginbotham, A. Sinitskii, J. R. Lomeda, A. Dimiev, B. K. Price and J. M. Tour, *Nature*, 2009, **458**, 872–876.

40 V. Sahu, V. K. Maurya, G. Singh, S. Patnaik and R. K. Sharma, *Mater. Des.*, 2017, **132**, 295–301.

41 A. Martín, P. Batalla, J. Hernández-Ferrer, M. T. Martínez and A. Escarpa, *Biosens. Bioelectron.*, 2015, **68**, 163–167.

42 S. Zhang, S. Tang, J. Lei, H. Dong and H. Ju, *J. Electroanal. Chem.*, 2011, **656**, 285–288.

43 Y. Fang, D. Zhang, Y. Guo, Y. Guo and Q. Chen, *Sensors Actuators, B Chem.*, 2015, **221**, 265–272.

44 C. Li, L. Wei, X. Liu, L. Lei and G. Li, *Anal. Chim. Acta*, 2014, **831**, 60–64.

45 F. Lucarelli, G. Marrazza, A. P. F. Turner and M. Mascini, *Biosens. Bioelectron.*, 2004, **19**, 515–530.

46 F. R. R. Teles and L. P. Fonseca, *Talanta*, 2008, **77**, 606–623.

47 T. I. Abdullin, O. V. Bondar, I. I. Nikitina, E. R. Bulatov, M. V. Morozov, A. K. Hilmutdinov, M. K. Salakhov and M. Çulha, *Bioelectrochemistry*, 2009, **77**, 37–42.

48 A. Bonanni, M. Pumera and Y. Miyahara, *Phys. Chem. Chem. Phys.*, 2011, **13**, 4980.

49 V. Sahu, S. Shekhar, R. K. Sharma and G. Singh, *ACS Appl. Mater. Interfaces*, 2015, **7**, 3110–3116.

View Article Online
DOI: 10.1039/C8TB01604F

50 A. C. Ferrari, *Solid State Commun.*, 2007, **143**, 47–57.

51 T. Ahmad, I. A. Wani, J. Ahmed and O. A. Al-Hartomy, *Appl. Nanosci.*, 2014, **4**, 491–498.

52 M. Das, C. Dhand, G. Sumana, a K. Srivastava, R. Nagarajan, L. Nain, M. Iwamoto, T. Manaka and B. D. Malhotra, 2011, 540–547.

53 C. Thiruppathiraja, S. Kamatchiammal, P. Adaikkappan, D. J. Santhosh and M. Alagar, *Anal. Biochem.*, 2011, **417**, 73–79.

54 M. Matsishin, A. Rachkov, A. Errachid, S. Dzyadevych and A. Soldatkin, *Sensors Actuators, B Chem.*, 2015, **222**, 1152–1158.

55 E. Torres-Chavolla and E. C. Alocilja, *Biosens. Bioelectron.*, 2011, **26**, 4614–4618.

56 M. Das, G. Sumana, R. Nagarajan and B. D. Malhotra, *Appl. Phys. Lett.*, 2010, **96**, 7–9.

57 A. Miodek, N. Mejri, M. Gomgnimbou, C. Sola and H. Korri-Youssoufi, *Anal. Chem.*, 2015, **87**, 9257–9264.

View Article Online
DOI: 10.1039/C8TB01604F

Reduced graphene oxide nanoribbon immobilized Gold nanoparticles based electrochemical DNA biosensor for detection of *Mycobacterium tuberculosis*

Navin Kumar Mogha, Vikrant Sahu, Raj Kishore Sharma, Dhanraj T. Masram

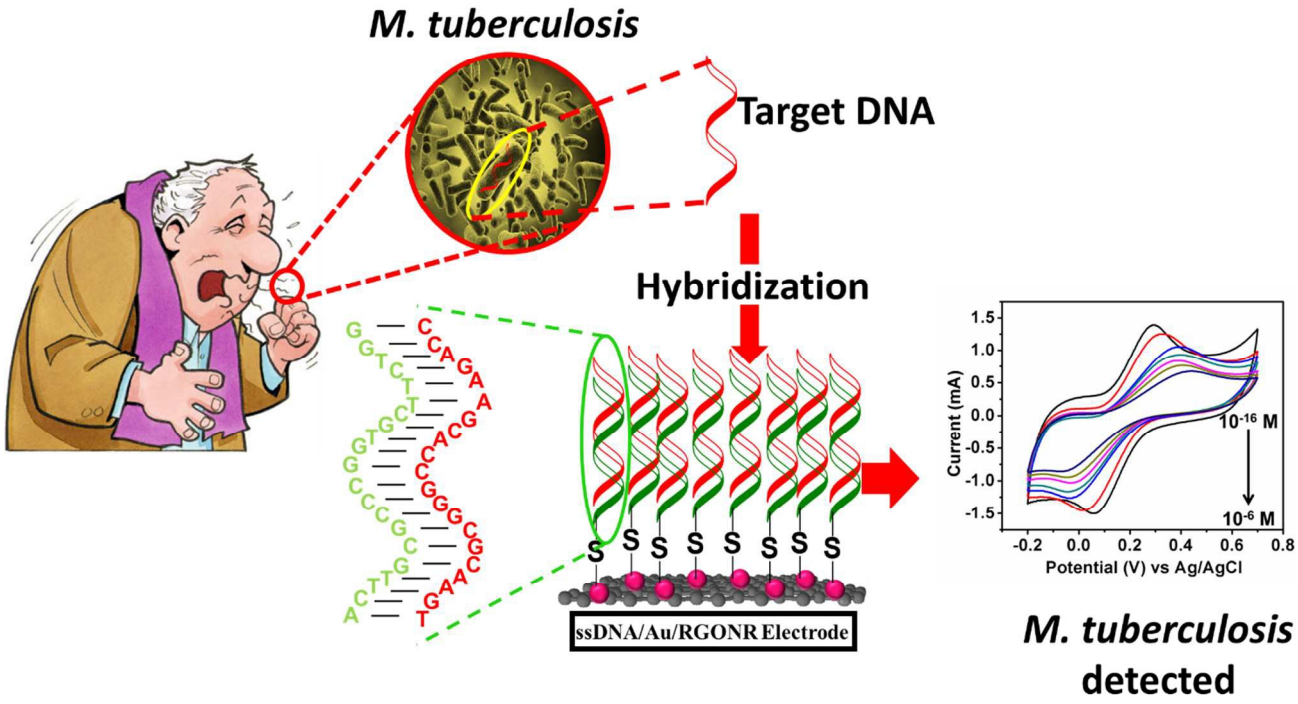

A DNA based biosensor is reported with very high specificity to *Mycobacterium tuberculosis* and detection limit much superior than already reported works